Title
Minimizing Decomposition of Vaporized Hydrogen Peroxide for Biological Decontamination of Galvanized Steel Ducting

Journal
Environmental Science and Technology, 42(15)

ISSN
0013-936X

Authors
Verce, Matthew F
Jayaraman, Buvaneswari
Ford, Timothy D
et al.

Publication Date
2008-08-01

DOI
10.1021/es702404g

Peer reviewed

Environ. Sci. Technol. **2008,** *42,* 5765–5771

Minimizing Decomposition of Vaporized Hydrogen Peroxide for Biological Decontamination of Galvanized Steel Ducting

MATTHEW F. VERCE,* [,†,‡]
BUVANESWARI JAYARAMAN, [§,|]
TIMOTHY D. FORD, [†,‡]
SCOTT E. FISHER, [†,‡] ASHOK J. GADGIL, [§] AND TINA M. CARLSEN [⊥]

Environmental Restoration, National Security Engineering, and Biosciences and Biotechnology Divisions, Lawrence Livermore National Laboratory, Livermore, California 94551, and Environmental Energy Technologies Division, Lawrence Berkeley National Laboratory, Berkeley, California 94720

Received September 24, 2007. Revised manuscript received April 8, 2008. Accepted May 7, 2008.

The behavior of vaporous hydrogen peroxide (VHP) was examined in clean, room-scale galvanized steel (GS) and polyvinylchloride-coated steel air ducts, to understand how it might be used to decontaminate larger ventilation systems. VHP injected into the GS duct decreased in concentration along the length of the duct, whereas VHP concentrations in the polyvinylchloride coated duct remained essentially constant, suggesting that VHP decomposed at the GS surface. However, decomposition was reduced at lower temperatures (~22 °C) and higher flow rates (~80 actual cubic meter per hour). A computational fluid dynamics model incorporating reactive transport was used to estimate surface VHP concentrations where bioaerosol contaminationislikelyto reside, and alsoshowed that VHP decomposition was enhanced at bends within the duct, comparedtostraightsections.Use of*G. stearothermophilus* indicators, in conjunction with model estimates, indicated that a concentration-contact time of ~100 mg/L H_2O_2(g)•min was required to achieve a 6 log reduction of indicator spores in clean GS duct, at 30 °C. When VHP is selected for building decontamination,thiswork suggeststhemost efficacious strategy may be to decontaminate GS ducting separately from the rest of the building, as opposed to a single decontamination event in which the ventilation system is used to distribute VHP throughout the entire building.

* Corresponding author phone: (925) 784-3948; e-mail: mfverce@ comcast.net. Mailing address: c/o William J. Smith, L-390, Lawrence Livermore National Laboratory, Livermore, CA 94551.

[†] Environmental Restoration Division, Lawrence Livermore Laboratory.

[‡] National Security Engineering Division, Lawrence Livermore Laboratory.

[§] Environmental Energy Technologies Division, Lawrence Berkeley National Laboratory.

[⊥] Biosciences and Biotechnology Division, Lawrence Livermore Laboratory.

[|] New address: ELORET Corp., NASA Ames Research Center, Mail Stop 215-1, Moffett Field, CA 94035-1000.

Introduction

The indoor environment can be contaminated with aerosol based viruses, bacteria, fungi, and their spores, either from natural occurring, outdoor environmental origins (*1*), or by their malicious introduction, such as the contamination resulting from the mailing of *B. anthracis* Ames strain spores in the United States in 2001 (*2*). The ventilation system inside a contaminated building is likely to become contaminated as well, either by bioaerosols in supply air brought into a building, or indirectly by reaerosolization (*3*) in rooms to which the system is connected. Once inside a ventilation system, bioaerosol transport can be influenced by a number factors, including size (*4, 5*), duct material (*5, 6*), and connectors and bends in the duct (*7*). Depending on its accessibility and value of associated hardware, demolition and disposal of a contaminated ventilation system may be prohibitively expensive. Therefore, a need exists to decon taminate high value ventilation systems *in situ*if they become contaminated with a bioaerosol.

Gaseous fumigants are a natural choice for decontami nating ducts, because they can be introduced at an accessible location and then allowed to permeate into the remote reaches of a ventilation system. Several fumigants can be considered for this purpose, including ozone (*8, 9*), paraform aldehyde (*10, 11*), methyl bromide (*12*), chlorine dioxide gas (*2, 13*), and vaporized hydrogen peroxide (VHP; ref (*14*)). The present work investigated the use of VHP because it kills a variety of biological contaminants found in the indoor environment, including vegetative bacteria and bacterial spores (*15*–*19*), fungi (*15, 20*), and viruses (*21*), decomposes into the innocuous end products water and molecular oxygen, and recently has been modified to decontaminate chemical warfare agents (*22*). Furthermore, it can be scaled up to decontaminate large buildings (*23, 24*), and was used to decontaminate some of the buildings after the incident in the United States in 2001 (*2*).

The overall objective of this work was to better understand the factors effecting the use of VHP to decontaminate ducting made of galvanized steel (GS), a material commonly used to construct ventilation systems in buildings. The specific tasks undertaken were to assess the effect of GS on VHP concen trations within a room-scale air duct; measure VHP con centrations as a function of operating parameters that practically can be adjusted during a decontamination event, including temperature, flow rate, and VHP injection rate; measure concentration-contact time (C•t) values required to kill biological indicators (BIs) of *Geobacillus stearother mophilus* spores, a surrogate for bioaerosol contamination, within the GS duct; develop and calibrate a computational fluid dynamics (CFD) model to predict VHP concentrations at any location within the duct;

use the CFD model to understand how bends in a GS duct effect VHP concentration; and illustrate how BI kill and CFD results can be used to estimate decontamination times for ducts.

Materials and Methods

Experimental Apparatus. Decontamination experiments were conducted in two adjacent rooms of a retrofitted construction trailer, housing a model duct run and required instrumentation, respectively. Separate duct runs were constructed of round, 6 in. (15.2 cm) diameter GS "snap duct" (obtained from a local building supply store; washed with soap and water prior to use) or polyvinylchloride (PVC)-coated steel duct (McMaster-Carr). A layout was chosen (Figure 1) to make the duct as long as practically possible

10.1021/es702404g CCC: $40.75 2008 American Chemical Society VOL. 42, NO. 15, 2008 / ENVIRONMENTAL SCIENCE & TECHNOLOGY [9] **5765** Published on Web 07/02/2008

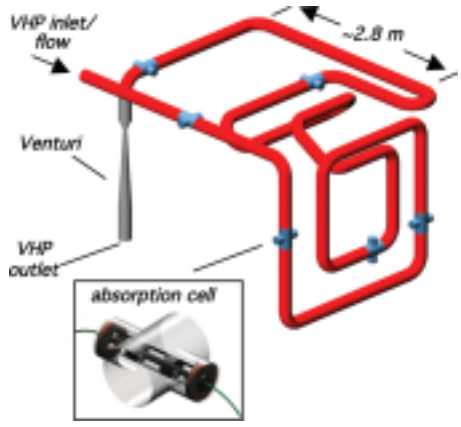

FIGURE 1. Schematic of experimental apparatus. Round GS and PVC-lined ducts were constructed and tested separately, but had essentially the same configuration shown here. Dimension shown indicates overall size of apparatus. Locations of near-infrared absorption cells for VHP and RH measurement (inset) were approximately 1, 4, 8, 13, 20, and 27 m from the inlet.

within the space of the test room. VHP produced by a STERIS VHP 1000 generator was introduced into one end of the duct, and VHP and water vapor concentrations were mea sured at six locations along the duct with near-infrared spectroscopy (Guided Wave model 412 process analyzer; ref (*25*)) by absorption cells (25 cm path length) placed normally to the duct's axis (inset, Figure 1) at each location. Relative humidity (RH) values were calculated by dividing measured water vapor concentrations by the saturation water vapor concentration, obtained from a published correlation with temperature (*26*). It was assumed that during decontamina tion a ventilation system's fans would not be used, so experiments were performed at flow rates of ~21-45 actual cubic meter per hour (acmh), much lower than those typically

where C_i and s_i are the steady state average and standard

found during normal building operation. Temperature at

$U_j\partial U_i$

$$\partial x_j\Big) + \partial\tau_{ij}$$

$$\partial x_{i+}\frac{\partial}{\partial x_j}\Big(\nu_{total}\partial U_i$$

each absorption cell was measured

$$\partial x_{j)} - \frac{1}{F}\frac{\partial p}{\partial x_j}(3)$$

were measured by a "machined convergent" type venturi placed at the end of the duct. Experiments were nearly isothermal, with temperatures decreasing by a maximum of 3 °C along the length of the duct.

Safety. Workers were protected from exposure to VHP by making the room containing the duct as airtight as practically

were solved to predict the steady-state airflow field in the

possible, and running experiments remotely from the adjacent room, which was maintained at a slightly higher relative air pressure. VHP concentrations in the adjacent room also were monitored by a Drager PAC III electrochemical detector alarmed at 1 ppmv.

VHP Profile Experiments. VHP concentration profiles were measured separately in GS and PVC-lined steel ducts

$U_j\frac{\partial k}{}$

deviation, respectively, of VHP concentrations or RH values from a given experiment (*27*).

C•t Values. C•t values were estimated with BIs containing approximately 2.5×10^6 *G. stearothermophilus* spores (Apex Laboratories, lot H0635) placed inside the GS duct, in the immediate vicinity of the first and fifth absorption cells (Figure 1). Ten BIs were used at each location per experiment, and three replicate experiments were performed for each exposure time. For convenience, BIs were taped to a plastic strip that was easily inserted into the duct (via ports cut into the duct at each location), which also positioned the BIs around the inner circumference of the duct, to mimic surface contamination. These tests were performed separately from those described above, but under the same nominal condi tions of 20 acmh and 30 °C. After a given exposure time, BIs were collected from the duct, placed aseptically into prepared tryptic soy broth tubes (PML Microbiologicals), incubated for 7 days at 55 °C, and then inspected visually for turbidity as a sign of growth.

Modeling VHP Fate and Transport. CFD simulation of the loss of VHP within the GS duct was performed using the commercial software STAR-CD (CD-Adapco) using the second-order Monotone Advection Reconstruction Scheme (*28*) and the SIMPLE algorithm (*29*). General boundary conditions included a laminar, plug flow velocity at the duct's entrance, isothermal walls, and setting the VHP mass entering the duct equal to the product of the experimentally measured flow rate and concentration at the first absorption cell (Figure 1). A computational grid consisting of 817,000 cells was constructed for the duct configuration shown in Figure 1. Local mesh refinement was carried out close to the walls, resulting in a maximum nondimensional normal distance (y^+) from the wall of 0.6. The finite volume formulation of the Reynolds Averaged Navier-Stokes equations

$$\frac{\partial U_j}{\partial x_j}) 0 (2)$$

by a thermistor (Omega, model THX400AP) protruding into the duct, and flow rates

duct. Turbulence was included via stress tensor elements (τ_{ij}, Supporting Information) determined by integrating the low-Reynolds-number turbulence model

$$\partial x_{j)}\frac{\partial}{\partial x_j}\Big(\nu_{total}\frac{\partial k}{}$$

$$\partial x_j) \frac{\partial}{\partial x_j}\left(\nu_{molec} + \nu_{turb}\right) \qquad P') -$$

$$U_j \frac{\partial \varepsilon}{\partial \varepsilon}$$

$$1.22 \qquad 1.92\left(1 - 0.3e^{-R_t^2}\right)\frac{\varepsilon^2}{k} \quad (5)$$

$$\partial x_j\Big) + \nu_{turb} P - \varepsilon \quad (4) \quad \partial x_j\Big) + \frac{\varepsilon}{k} 1.44 \upsilon_{turb}(P +$$

at various initial VHP concentrations entering the duct, flow rates, and temperatures (Table 1). The liquid hydrogen peroxide sterilant vaporized by the STERIS VHP 1000 generator was either a 35% solution (Vaprox , STERIS), or a 14% solution (obtained by dilution) to achieve lower VHP concentrations. Vaporization and flow rates were chosen to avoid condensation of VHP and water vapor during experi ments. All experiments were run for a minimum of four hours (six hours was common), to ensure steady state values were reached throughout the entire duct. For each set of conditions tested, three experiments were performed on separate days, and VHP and RH concentrations were reported as a weighted average calculated by

$$\sum_i C_i \qquad s_i^2 \Big/ \sum \frac{1}{i} s_{i2} \quad (1)$$

all the way to the wall of the duct (as opposed to assuming a wall function). Lastly, the VHP concentrations were predicted for a given airflow field by solving the transport equation

$$\partial x_{j+} \frac{\partial}{\partial x_j}\left(C V_{mj} + u_j' C'\right)) S \quad (6)$$

$$U_j \frac{\partial C}{}$$

where S is a sink term due to VHP decomposition, which was set equal to

$$S) - \frac{K_1 C}{K_2 + C} \quad (7)$$

in the first layer of cells adjacent to the wall, and zero everywhere else. The mixed order form of eq 7 was suggested by data collected at different initial VHP concentrations (see

TABLE 1. Summary of Experimental Conditions Tested, and Corresponding Amounts of VHP Decomposition in GS Duct for Each Condition (VHP Concentrations, RH Values, and Flow Rates Are Reported As Weighted Averages Calculated with Eq 1 (± Standard Deviation) from Three Experiments Performed on Different Days; Temperatures Are Simple Averages between First and Last Absorption Cells; Percent VHP Decomposition Values Were Computed from Mass Balance Calculations As Described in Text)

experimental conditions							
first absorption cell		last absorption cell					
VHP (mg/L)	RH (%)	VHP (mg/L)	RH (%)	avg temp[a] (°C)	H_2O_2 (l) sterilant (%w/w)	H_2O_2 (l) vap rate[b] (g/min) flow rate (acmh)[c]	VHP decomp[d] (mass %)
experiments at different initial concentrations (corresponds to data in Figure 2a)							
0.36 (0.01	9.5 (0.1	0.02 (0.002	10.5 (0.1	29.9 (0.8	14 1.0	19.6 (0.2	95.2 0.58 (0.01
14.0 (0.1	0.06 (0.004	14.8 (0.1	29.8 (0.8	14 1.5	20.7 (0.2	90.1 1.12 (0.03	
8.4 (0.1	0.20 (0.01	10.5 (0.1	30.2 (0.7	35 1.2	19.7 (0.2	84.2	
experiments at different flow rates (corresponds to data in Figure 3)							
0.53 (0.01	10.4 (0.2	0.15 (0.01	16.8 (0.2	31.1 (1.1	35 1.2	46.6 (0.3	71.3 0.52 (0.01
20.4 (0.3	0.23 (0.01	17.1 (0.3	29.7 (0.2	35 2.1	77.9 (0.3	60.2	
experiments at different temperatures (corresponds to data in Figure 4)							
1.11 (0.01	12.2 (0.2	0.50 (0.01	12.8 (0.2	21.8 (0.6	35 1.1	19.4 (0.2	58.4 1.16 (0.16
6.8 (0.1	0.02 (0.003	7.1 (0.2	37.8 (0.4	35 1.4	19.9 (0.2	98.6	

[a] Average temperature between first and last absorption cells. [b] Vaporization rate of H_2O_2 (l) sterilant. [c] Actual cubic meters per hour. [d] VHP decomposition in GS duct.

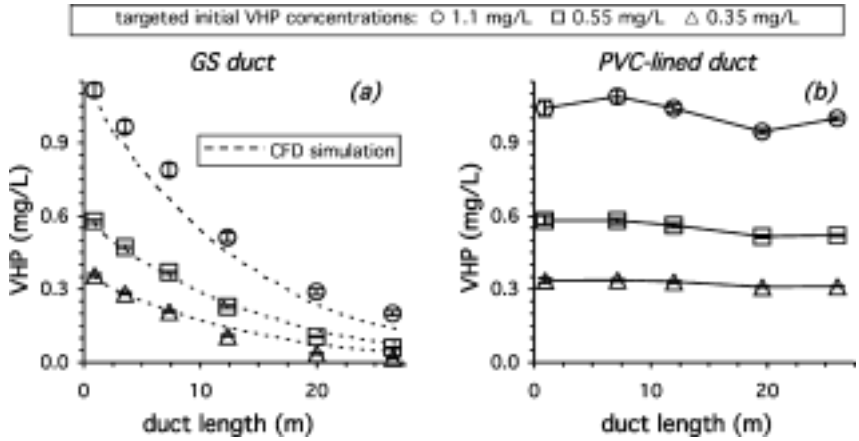

FIGURE 2. Effect of initial VHP concentration entering duct on VHP profiles in GS (a) and PVC-lined steel (b) ducts, respectively, and CFD predictions of VHP concentrations in GS duct (dotted lines in panel a). Nominal conditions were ~21 acmh and ~30 °C; see Table 1 for exact values. Each symbol is a weighted average (calculated via eq 1) of VHP concentrations from a given absorption cell ((standard deviation as error bars) for triplicate experiments performed on separate days. Data from the PVC-lined duct were not modeled with CFD and therefore are connected with solid lines (b).

Results), which indicated a uniform loss rate at the highest concentrations tested, and a first order loss at lower concentrations. Several simulations of each VHP data set were performed, until one set of values for K_1 and K_2 was obtained that resulted in an acceptable root-mean-square error. All terms in the above equations are summarized in Nomenclature.

Results

Qualitative Effect of VHP on GS. Oxidative damage to the GS duct was minimal, even after performing more than 100 experiments over a one year period. A visual examination of the GS duct when it was dismantled revealed a patina on surfaces in the immediate vicinity of where VHP was introduced, but most of the duct had a mildly dulled or hazed appearance, compared to GS not exposed to VHP.

Duct Material and Process Parameter Effects. Repro ducible data from the GS duct were obtained after initial passivation of the GS duct during several preliminary experiments (data not shown). Results of experiments performed at different VHP mass loading rates (or equiva lently, different initial VHP concentrations entering the duct) with GS and PVC-lined steel ducts are shown in Figure 2. As can be seen, VHP concentrations decreased markedly along the length of the GS duct (Figure 2a), but were essentially constant in the PVC-lined duct tested under the same nominal conditions (Figure 2b). VHP concentrations in the GS duct also were dependent on flow rate (Figure 3) and temperature (Figure 4). To determine the effect of each parameter, the percent VHP loss was calculated as the ratio of VHP mass exiting the duct to the total VHP mass vaporized by the generator during each set of experiments (Table 1). As can be seen, the highest flow rate (~78 acmh) and the lowest temperature (~22 °C) tested led to the smallest percent losses within the GS duct. Increasing the initial VHP concentration with other parameters held constant also minimized VHP loss, but not to the same extent (Table 1). VHP losses were the largest at the lowest initial concentration and highest temperature tested (Table 1). RH values in all experiments were low (e.g., < 30%), and essentially constant over the length of the duct for a given experiment (Table 1; Supporting Information).

VHP Decomposition Rates. The attenuation of VHP in the GS duct, but minimal attenuation in the PVC-lined duct under the same conditions, suggested that the GS was catalyzing the decomposition of VHP at the surfaces of the

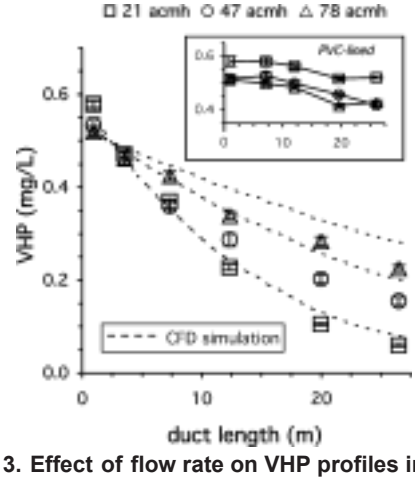

FIGURE 3. Effect of flow rate on VHP profiles in GS and PVC-lined steel (inset) ducts, and CFD predictions of VHP concentrations in GS duct (dotted lines). Nominal conditions were ~30 °C and ~0.55 mg/L at the first absorption cell; see Table 1 for exact values. Data at 21 acmh (○) are reproduced from Figure 2a for ease of comparison. See caption of Figure 2 for additional remarks.

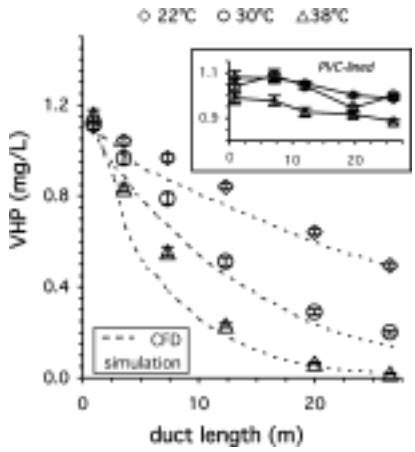

FIGURE 4. Effect of temperature on VHP profiles in GS and PVC-lined steel (inset) ducts, and CFD predictions of VHP concentrations in GS duct (dotted lines). Nominal conditions were ~21 acmh and ~1.1 mg/L at the first absorption cell; see Table 1 for exact values. Data at 30 °C (O) are reproduced from Figure 2a for ease of comparison. See caption of Figure 2 for additional remarks.

TABLE 2. Values of K_1 and K_2 (Eq 7), and Surface Area Normalized Decomposition Rates (K_A) of VHP in GS Duct, As a Function of Temperature Tested

avg. temp (°C)	K_1 (mg/L/sec)	K_2 (mg/L)	K_A (nmol/min/cm^2)[a]
21.8	4.0	1.9	40
30.2	9.0	1.3	97
37.8	16	0.8	167

[a] Nanomoles VHP/min/cm^2 of GS duct.

duct. To test this hypothesis, the three-dimensional CFD model incorporating reaction at the GS surface was fitted to the VHP data (dotted lines in Figures 2 and 4). Due to the temperature sensitivity of VHP decomposition, the model was fit separately to data from each temperature tested (Table 2). The coefficients at ~30 °C were determined by fitting data at lower (Figure 2a) and higher (Figure 3) flow rates simultaneously to obtain one representative set of coefficients for this temperature, as opposed to fitting them separately. The agreement between measured and CFD-predicted VHP

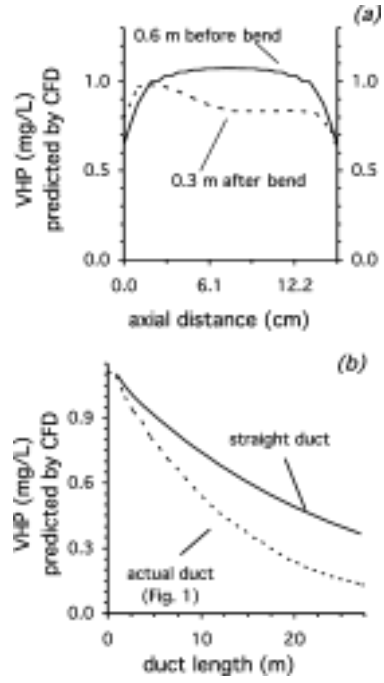

FIGURE 5. Effect of bends in GS duct on VHP concentration. Panel (a) shows the VHP concentration profile estimated by CFD at 0.6 m before (solid line) and 0.3 m after (dotted line) the first bend in the duct. The abscissa in (a) is the axial distance across the duct. Panel (b) shows the overall effect of bends, comparing a CFD simulation of the actual GS duct tested (dotted line; reproduced from Figure 2a) with a simulation of a straight duct with no bends (solid line) of the same total length.

concentrations was reasonable for all temperatures except ~30 °C, for which agreement was better at lower flow rates (e.g., Figure 2a) than at higher ones (Figure 3).

Surface area normalized decomposition rates were es timated by dividing the VHP loss rate, given by eq 7, by the surface area of the grid cell at a particular location. The largest decomposition rates observed in this study (Table 2) were estimated at the beginning of the duct where VHP sur face concentrations, and therefore decomposition, were the highest. These rates may not be maximal, however, because some experiments were initiated at VHP concentrations near or below the value of K_2 (Table 2), implying decomposition rates (e.g., eq 7) may not have reached maximum values.

Effect of Bends on VHP Concentration. Once values for K_1 and K_2 were obtained, the CFD model was used to understand the effect of bends on VHP concentration within the GS duct. Using the first bend as an example, the CFD model showed the velocity profile (see Supporting Informa tion) and VHP concentration profile exiting the bend (Figure 5a) were altered, and of a lower average value, compared to regions of straight duct with fully developed flow. This is consistent with the general expectation that a change in flow direction induced by bends enhances mass and heat transfer (*30, 31*), in this case enhancing the reaction of VHP at the GS surface. VHP loss is enhanced at every bend, so that after ~1.5m the actual duct tested was predicted to have lower concentrations than a straight duct (Figure 5b) of equal length. A similar phenomena will occur in other duct configurations, as the fluid flow containing the VHP under goes a change in direction at each bend it encounters.

Surface VHP Concentrations. One straightforward out come of a surface-catalyzed decomposition process is a

decrease in VHP concentrations contacting the surface. Again using the first bend in the GS duct as an example, the VHP concentrations contacting the walls of the duct (e.g., at axial distances 0 and 15.24 cm, Figure 5a) were appreciably lower

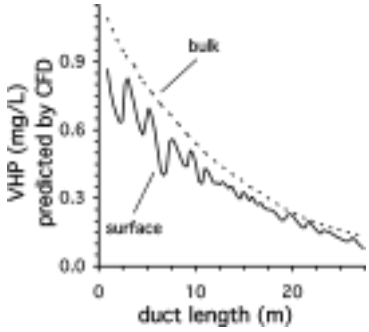

FIGURE 6. Comparison between CFD-predicted bulk and surface concentrations in the GS duct. The surface concentration (solid line) is for an arbitrary line run along the length of the duct; the bulk concentration (dotted line) is reproduced from Figure 2a. The oscillations in surface concentrations (solid line) are due to locally lower VHP concentrations experienced on the inner edge of some bends, and locally higher concentrations on the outer edge of other bends.

than the bulk concentration at this location. This is illustrated further in Figure 6, which shows the surface concentrations were predicted to be lower than bulk concentrations throughout the entire duct. The distinction between bulk and surface concentrations is important, because bioaerosols settling on the interior of ducts (*5, 6*) will experience lower surface VHP concentrations, as opposed to higher, bulk concentrations reported by most commercial detectors.

C•t Values and Estimated Decontamination Times. C•t values at the first and fifth absorption cells (Figure 1) were estimated as the product of the exposure time required to kill BIs and the surface VHP concentration (obtained by CFD) at each location. The results are shown in Figure 7, which indicates a minimum C•t value of 83 mg/L•min (0.925 mg/L•90 min) was required to kill all BIs placed at the first absorption cell (Figure 7a), whereas a value greater than 100 mg/L•min (0.185 mg/L•540 min) may have been required at the fifth absorption cell (Figure 7b). The positive result at the fifth absorption cell at 100 mg/L•min (Figure 7b) was due to the growth of one BI out of thirty. These C•t values correspond to a 6 log reduction of indicator organisms under the conditions tested, because the BIs had a burden >2 × 10^6 spores.

One way to estimate the time required to decontaminate an air duct is to determine the time at which the entire inner surface of the duct exceeds a given C•t value. For this approach, CFD can provide the VHP concentrations contacting the surface where spores would likely reside, and the C•t value used must be representative of the conditions inside the duct. This is illustrated in Figure 8 for the GS duct tested, which compares the decontamination time for experiments performed at the highest flow rate (open triangles, Figure 3) with that of experiments performed at the highest initial concentration (open circles, Figure 2a). As can be seen, conditions associated with the highest flow rate tested (curve a, Figure 8) decontaminated the GS duct approximately three times faster than those associated with the highest initial concentration (curve b, Figure 8). This illustration assumed a constant C•t value (e.g., "Chick-Watson" or "toxic load" exponent equal to 1) of 100 mg/L•min determined from BI experiments (above). The two curves in Figure 8 cross because the VHP concentrations at the highest flow rate tested initially were lower in the first ~12 m of the duct (Figure 2a), but then were higher in the remaining length of the duct, compared to experiments at the highest initial concentration tested (Figure 3).

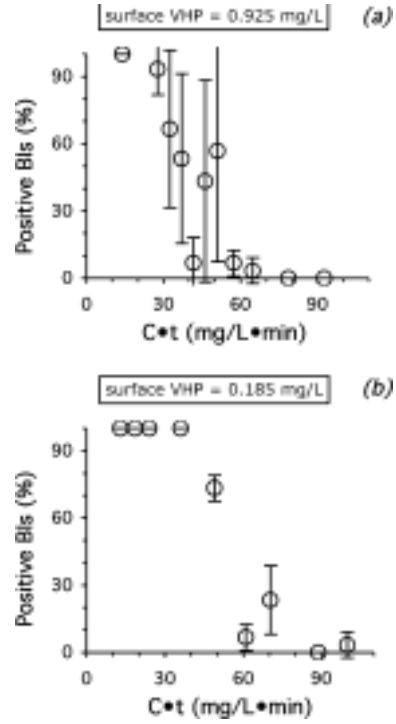

FIGURE 7. Kill of *G. stearothermophilus* BIs placed in the immediate vicinity of the first (a) and fifth (b) absorption cells in the GS duct, at nominal conditions of ~30 °C and ~20 acmh flow rate. Results are expressed as the percent of BIs that were positive for growth at the corresponding C•t value. Symbols are averages ((standard deviation as error bars) from triplicate experiments in which 10 BIs were used per experiment. Surface VHP concentrations given in each panel were obtained from CFD.

	Initial VHP (mg/L)	Avg. Temp. (°C)	Flow Rate (acmh)
a	0.52	29.7	77.9
b	1.1	30.2	19.7

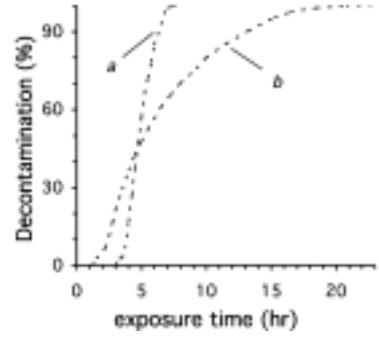

FIGURE 8. Estimated fractional decontamination of the GS duct, for the highest flow rate (curve a) and highest initial VHP concentration (curve b) tested. Decontamination was estimated as the fraction of the duct's surface that exceeded a C•t value of 100 mg/L•min for a given exposure time step.

Discussion

The observations of decreasing VHP concentrations along the length of the GS duct under a variety of conditions, but

essentially constant VHP concentrations along the length of the PVC-lined duct, strongly indicate that VHP undergoes a surface-catalyzed, heterogeneous decomposition as it passes through GS ducting. Clearly, the loss observed in the GS duct was not due to homogeneous decomposition of VHP, which occurs only at temperatures greater than 400 °C (*32*). Heterogeneous decomposition of VHP has been reported

qualitatively at near-ambient temperatures (*33, 34*). VHP decomposition rates also have been measured at temper atures between 110 and 250 °C, and ranged between 1 μmole H_2O_2/min/cm^2 for glass to greater than 100 μmole H_2O_2/ min/cm^2 for electropolished stainless steel (*35*). Although the decomposition rates for GS duct reported in the present study at ambient temperatures (40-167 nmol H_2O_2/min/ cm^2; Table 2) are at least 2 orders of magnitude smaller than those reported at higher temperatures, the very large surface area of a typical duct system is likely to cause a substantial loss of VHP that will impact decontamination. VHP is not unique in its reaction and depletion at surfaces, however. Other fumigants, including chlorine dioxide (*13*) and ozone (*36, 37*) also are consumed by surfaces found in the indoor environment, although the effect of GS on these other fumigants apparently has not yet been reported.

Though VHP decomposition is catalyzed by GS surfaces, the results presented here show it can be minimized by the choice of operating conditions during decontamination. Temperature, flow rate, and initial concentration each effected the fraction of VHP mass decomposed, with tem perature and flow rate having the most beneficial effect over the ranges tested (Table 1). Clearly, lower temperatures slowed the kinetics of VHP decomposition. The effect of temperature does not seem attributable to water vapor displacing VHP at the GS surface, because RH values for all experiments were low. Specifically, the RH values for experiments performed at different temperatures were nearly constant, and within 10% throughout the entire duct (Table 1; Supporting Information). It should be noted that lowering the temperature to decrease VHP decomposition also may slow the kinetics of VHP killing spores, as observed in liquid H_2O_2 solutions (*38, 39*). Higher flow rates apparently acted by reducing the residence time within the duct to react with the GS surface. Higher flow rates are easily produced with large blowers, but would require a larger VHP generator (*23*) to maintain sporicidal concentrations. The fact that higher flow rates, which also increase turbulent transport of VHP to the GS surface, did not increase the amount of the VHP consumed, suggests the fitted coefficients in Table 2 largely are independent of transport effects unique to this experi ment, and capture the kinetics of VHP decomposition at the GS surface tested. Of course, to develop a predictive engineering capability for duct decontamination, kinetic coefficients for a variety of indoor surfaces, including surfaces soiled with typical indoor dust and grime, and a variety of temperatures and RH values, should be obtained.

Though the CFD model developed is specific to the duct system tested here, it yielded information that is transferable to the decontamination of other GS ducts. First, it yielded quantitative information about the kinetics of VHP decom position at the GS surface. As discussed above, the kinetic coefficients obtained are largely independent of flow and transport characteristics specific to this experiment, and become a way to compare the results of this work with other studies of VHP in ducts, as they become available. The CFD model also revealed two qualitative effects-the enhanced loss of VHP due to changes in flow direction at bends, and the difference between bulk and surface VHP concentrations-which will be manifested to some degree in other duct systems. It is recognized that CFD cannot be applied to every ventilation system that may require de contamination. Rather, this work suggests that CFD analysis of a limited number of additional experiments, involving different duct materials, geometries, and flow rates, could provide average reaction rates that would reasonably predict decontamination in a wide variety of ventilation systems.

The present work attempted to capture the effect of VHP decomposition on biological decontamination by placing BIs of *G. stearothermophilus* spores inside the GS duct. *G.*

stearothermophilus spores are more resistant to VHP than many bacterial (*15*–*17*) and mold (*15*) spores. *G. stearother mophilus* spores also were more resistant to VHP than spores of the highly virulent *B. anthracis* Ames strain, when both were inoculated onto coupons made of galvanized steel (*18*). Clearly, use of BIs in this manner is different from killing bioaerosol contaminants deposited in an aged duct. The GS duct used in the present study was new and passivated, whereas functioning ventilation systems contain dust, grime, and other materials that will most likely exert an additional oxidative demand for VHP. Therefore, the C•t values pre sented here very likely underestimate actual values required to decontaminate aged GS duct in a building.

Minimizing decomposition of VHP will aid in the de contamination of GS duct, whether contaminated by naturally occurring bioaerosols from the outdoor environment, or by a biological warfare agent after a spectacular event. Other favorable characteristics of VHP, such as its effectiveness at lower RH values and minimal corrosivity when compared to chlorine dioxide (*40*), make it an attractive fumigant for high value or inaccessible ventilation systems for which replace ment or demolition would be prohibitively expensive. For these cases, VHP decomposition could be overcome by a choice of operating parameters described here, and by isolating the ventilation system and decontaminating it separately from the rest of the building. This approach was used during the successful decontamination of the General Services Administration's Building 410 with VHP (*41*), after that facility was contaminated with *B. anthracis* spores in 2001, and could prove equally useful for other facilities contaminated with naturally occurring bioaerosols.

Acknowledgments

This work was performed under the auspices of the following: the U.S. Department of Energy by University of California at Lawrence Livermore National Laboratory (experiments; Contract W-7405-Eng-48) and Lawrence Berkeley National Laboratory (modeling; Contract DE-AC02-05CH11231), both of which were funded by the Department of Homeland Security; and a Cooperative Research and Development Agreement with Strategic Technology Enterprises Inc., a subsidiary of STERIS Corp. Diana Warden helped perform initial duct experiments, Michael Feldman assisted with CFD modeling, and Lianna Balser assisted with BI experiments. George Metzger provided valuable assistance with venturi flow measurements.

Appendix

C concentration of VHP (mg/L)

C_i steady state average VHP concentration or RH value

from a given experiment

C' fluctuating components of concentration C•t Product of VHP concentration and exposure time (mg/L•min)

K_a Surface area normalized VHP decomposition rate (nmol/min/cm^2)

K_1 zeroth order VHP decomposition constant (mg/L/ sec)

K_2 VHP concentration at half maximum rate (mg/L) k turbulent kinetic energy (m^2/sec^2)

P production of turbulent kinetic energy k, by mean velocity gradients

P' near-wall turbulence energy dissipation p pressure (Pa)

R_t turbulent Reynolds number

s_i standard deviation of VHP concentration from a given experiment

t time (sec)

u'_i fluctuating velocity component (m/sec) U_i mean velocity component (m/sec)

$V_{m,j}$ diffusion velocity component (m/sec) x_i Cartesian coordinate (i) 1, 2, 3) (m) y^+ non-dimensional normal distance from the wall ε turbulent dissipation rate (m^2/sec^3)

v_{total} total kinematic viscosity (m^2/sec)

v_{turb} turbulent kinematic viscosity (m^2/sec) v_{molec} molecular kinematic viscosity (m^2/sec) F density (kg/m^3)

τ_{ij} components of stress tensor (Pa)

Supporting Information Available

Additional details of the experimental apparatus, CFD modeling, RH data, and the effect of bends on VHP decomposition. This material is available free of charge via the Internet at http://pubs.acs.org.

Literature Cited

(1) Jones, A. P. Indoor air quality and health. *Atmos. Environ.* **1999**, *33* (28), 4535–4564.

(2) Sharp, R. J.; Roberts, A. G. Anthrax: the challenges for decon tamination. *J. Chem. Technol. Biotechnol.* **2006**, *81*, 1612–1625.

(3) Weis, C. P.; Intrepido, A. J.; Miller, A. K.; Cowin, P. G.; Durno, M. A.; Gebhardt, J. S.; Bull, R. Secondary aerosolization of viable *Bacillus anthracis* spores in a contaminated US Senate Office. *JAMA* **2002**, *288* (22), 2853–2858.

(4) Sippola, M. R.; Nazaroff, W. W. Modeling particle loss in ventilation ducts. *Atmos. Environ.* **2003**, *37*, 5597–5609. (5) Sippola, M. R.; Nazaroff, W. W. Experiments measuring particle deposition from fully developed turbulent flow in ventilation ducts. *Aerosol Sci. Technol.* **2004**, *38*, 914–925.

(6) Krauter, P.; Biermann, A.; Larsen, L. D. Transport efficiency and deposition velocity of fluidized spores in ventilation ducts. *Aerobiologia* **2005**, *21*, 155–172.

(7) Sippola, M. R.; Nazaroff, W. W. Particle deposition in ventilation ducts: connectors, bends, and developing turbulent flow.*Aerosol Sci. Technol.* **2005**, *39*, 139–150.

(8) Currier, R. P.; Torraco, D. J.; Cross, J. B.; Wagner, G. L.; Gladden, P. D.; Vanderberg, L. A. Deactivation of clumped and dirty spores of *Bacillus globigii*. *Ozone: Sci. Eng.* **2001**, *23* (4), 285–294.

(9) Aydogan, A.; Gurol, M. D. Application of gaseous ozone for inactivation of *Bacillus subtilis* spores. *J. Air Waste Manage.* **2006**, *56* (2), 179–185.

(10) Munro, K.; Lanser, J.; Flower, R. A comparative study of methods to validate formaldehyde decontamination of biological safety cabinets. *Appl. Environ. Microbiol.* **1999**, *65* (2), 873–876.

(11) Canter, D. A.; Gunning, D.; Rodgers, P.; O'Connor, L.; Traunero, C.; Kempter, C. J. Remediation of *Bacillus anthracis* contamina tion in the U.S. Department of Justice Mail Facility. *Biosecur. Bioterror.* **2005**, *3* (2), 119–127.

(12) Juergensmeyer, M. A.; Gingras, B. A.; Scheffrahn, R. H.; Weinberg, M. J. Methyl bromide fumigant lethal to *Bacillus anthracis* spores. *J. Environ. Health* **2007**, *69* (6), 24–26.

(13) Han, Y.; Applegate, B.; Linton, R. H.; Nelson, P. E. Decontamination of *Bacillus thuringiensis* spores on selected surfaces by chlorine dioxide gas. *J. Environ. Health.* **2003**, *66* (4), 16–20.

(14) Cummings, A. L.; Childers, R. W.; Mielnik, T. J. Flow-through vapor phase sterilization system;US Patent no. 4,909,999; 1990.

(15) Rickloff, J. R.; Orelski, P. A. Resistance of various microorganisms to vaporized hydrogen peroxide in a prototype tabletop sterilizer. In*Proceedings of the 89th AnnualMeeting of the American Society ofMicrobiology*; American Society for Microbiology: Washington, DC, 1989; Vol. 15, p 21.

(16) Klapes, N. A.; Vesley, D. Vapor-phase hydrogen peroxide as a surface decontaminant and sterilant. *Appl. Environ. Microbiol.* **1990**, *56* (2), 503–506.

(17) Johnston, M. D.; Lawson, S.; Otter, J. A. Evaluation of hydrogen peroxide vapour as a method for the decontamination of surfaces contaminated with *Clostridium botulinum* spores. *J. Microbiol. Meth.* **2005**, *60* (3), 403–411.

(18) Rogers, J. V.; Sabourin, C. L. K.; Choi, Y. W.; Richter, W. R.; Rudnicki, D. C.; Riggs, K. B.; Taylor, M. L.; Chang, J. Decon tamination assessment of *Bacillus anthracis*, *Bacillus subtilis*, and *Geobacillus stearothermophilus* spores on indoor surfaces using a hydrogen peroxide gas generator. *J. Appl. Microbiol.* **2005**, *99*, 739–748.

(19) Kokubo, M.; Inoue, T.; Akers, J. Resistance of common envi ronmental spores of the genus *Bacillus* to vapor hydrogen peroxide. *PDA J. Pharm. Sci. Technol.* **1998**, *52* (5), 228–231.

(20) Rij, R. E.; Forney, C. F. Phytotoxocity of vapour phase hydrogen peroxide to Thompson Seedless grapes and *Botrytis cinerea* spores. *Crop Prot.* **1995**, *14* (2), 131–135.

(21) Heckert, R. A.; Best, M.; Jordan, L. T.; Dulac, G. C.; Eddington, D. L.; Sterritt, W. G. Efficacy of vaporized hydrogen peroxide against exotic animal viruses. *Appl. Environ. Microbiol.* **1997**, *63* (10), 3916–3918.

(22) Wagner, G. W.; Sorrick, D. C.; Procell, L. R.; Brickhouse, M. D.; McVey, I. F.; Schwartz, L. I. Decontamination of VX, GD, and HD on a surface using modified vaporized hydrogen peroxide. *Langmuir* **2007**, *23* (3), 1178–1186.

(23) Edwards, S. J.; Geist, S. G.; Steen, P. A. Multiple flashpoint vaporization system; US Patent No. 6,077,480; 2000. (24) Brickhouse, M. D.; Turetsky, A.; McVey, I. F. *Decontamination of CBW Agents by mVHP: Demonstration of the CBW Decon tamination of a Building using mVHP*; Edgewood Chemical Biological Center Technical Report ECBC-TR-470S; 2005. (25) Adams, D.; Brown, G. P.; Fritz, C.; Todd, T. T. Calibration of a near-infrared (NIR) H_2O_2 vapor monitor. *Pharm. Eng.* **1998**, *18* (4), 66–85.

(26) Manatt, S. L.; Manatt, M. R. R. On the analyses of mixture vapor pressure data: the hydrogen peroxide/ water system and its excess thermodynamic functions. *Chem.- Eur. J.* **2004**, *10* (24), 6540–6557.

(27) Bevington, P. R.; Robinson, D. K. *Data Reduction and Error Analysis for the Physical Sciences*, 2nd ed; McGraw-Hill: New York, 1992; p 59.

(28) Asproulis, P. N. High resolution numerical predictions of hypersonic flows on unstructured meshes; Ph.D Dissertation, Imperial College, Dept. of Aeronautics, London, 1994.

(29) Patankar, S. V. *Numerical Heat Transfer and Fluid Flow*; Hemisphere: Washington DC, 1980.

(30) Naphon, P.; Wongwises, S. A review of flow and heat transfer characteristics in curved tubes. *Renew. Sust. Energy Rev.* **2006**, *10* (5), 463–490.

(31) Berger, S. A. Flow and heat transfer in curved pipes and tubes; AIAA 1991-0030; Presented at 29th Aerospace Sciences Meeting, 1991; pp 119.

(32) Satterfield, C. N.; Stein, T. W. Homogeneous decomposition of hydrogen peroxide vapor. *J. Phys. Chem. (U.S.)* **1957**, *61* (5), 537–540.

(33) Hart, A. B.; Ross, R. A. Catalytic decomposition of hydrogen peroxide vapour by equimolar mixed oxides. *Nature* **1962**, *193* (4821), 1175–1177.

(34) Hart, A. B.; McFadyen, J.; Ross, R. A. Solid-oxide-catalyzed decomposition of hydrogen peroxide vapour. *T. Faraday Soc.* **1963**, *59* (486), 1458–1469.

(35) Satterfield, C. N.; Stein, T. W. Decomposition of hydrogen peroxide vapor on relatively inert surfaces.*Ind. Eng. Chem.* **1957**, *49* (7), 1173–1180.

(36) Morrison, G. C.; Nazaroff, W. W.; Cano-Ruiz, J. A.; Hodgson, A. T.; Modera, M. P. Indoor air quality impacts of ventilation ducts: ozone removal and emissions of volatile organic com pounds. *J. Air Waste Manage.* **1998**, *48* (10), 941–952.

(37) Zhao, P.; Siegel, J. A.; Corsi, R. L. Ozone removal by HVAC

filters. *Atmos. Environ.* **2007**, *41* (15), 3151–3160.
(38) Swartling, P.; Lindgren, B. The sterilizing effect against *Bacillus subtilis* spores of hydrogen peroxide at different temperatures and concentrations. *J. Dairy Res.* **1968**, *35*, 423–428.
(39) Toledo, R. T.; Escher, F. E.; Ayres, J. C. Sporicidal properties of hydrogen peroxide against food spoilage organisms. *Appl. Microbiol.* **1973**, *26* (4), 592–597.
(40) Gordon, G.; Rosenblatt, A. A. Chlorine dioxide: the current state of the art. *Ozone: Sci. Eng.* **2005**, *27* (3), 203–207.
(41) Strategic Technology Enterprises Inc. *VHP fumigation of GSA Building 410;* 2003, provided by Iain F. McVey as a personal communication.

ES702404G